Appl. Phys. B 77, 361–368 (2003)
DOI: 10.1007/s00340-003-1224-5

Applied Physics B
Lasers and Optics

S. JUODKAZIS[1,2]✉
A.V. RODE[3]
E.G. GAMALY[3]
S. MATSUO[1,2]
H. MISAWA[2,4]

Recording and reading of three-dimensional optical memory in glasses

[1] Ecosystem Engineering Department, The University of Tokushima, 2-1 Minamijosanjima, Tokushima 770-8506, Japan
[2] Core Research for Evolution Science & Technology (CREST), Japan Science & Technology Corporation (JST), Japan
[3] Laser Physics Center, Australian National University, Canberra ACT 0200, Australia
[4] Research Institute for Electronic Science, Hokkaido University, Sapporo 060-0812, Japan

Received: 2 February 2003/Revised version: 12 May 2003
Published online: 8 August 2003 •

ABSTRACT We report on three-dimensional (3D) optical memory recording and reading in glass by femtosecond pulses. Optically induced dielectric breakdown of glass is a mechanism of recording. The formulae of dielectric breakdown presented are applicable, in principle, for any crystalline or amorphous dielectric material. Scaling dependences of the probabilities of multi-photon and impact ionization are given. The measured threshold of an in-bulk dielectric breakdown of silica was reproduced numerically by implementing the ionization potential of Si (8.15 eV) for calculations. Exact measures of focal spot size and pulse duration at the focus allowed us to evaluate the intensity of a pulse during recording of 3D optical memory bits with high accuracy. The readout of the 3D optical memory was carried out by the white-light continuum generated from the previously damaged sites (recorded memory bits). The mechanism of the readout was a four-photon parametric interaction.

PACS 42.65.Jx; 42.65.Ky; 42.70.Ce; 42.79.Vb

1 Introduction

Technology used for the production of semiconductor microchips will soon enable industry-grade fabrication with a smallest feature size of 100 nm. One of new optical memory formats, the blue-laser DVD (for a digital versatile disk) format, agreed upon in February 2002, features up to 27 GBytes of memory on one side of a single 12-cm disk, nearly six times the capacity of current 4.7 GByte disks. However, these are the achievements of two-dimensional (2D) microfabrication. Developing technologies of three-dimensional (3D) fabrication which would enable us to achieve a minimum feature size of 0.1–1 μm is still a challenge, and attracts an increasing interest. Tools for manipulation, handling, and fabrication on this scale are important for the future of nano-/microfabrication and assembling techniques as well. There the interest is also prompted by the efforts to bridge differences in current microtechnology and the bio-world, where the most crucial processes occur on this particular length scale of 0.1–1 μm. In the field of optical memories, a transition from 2D towards the 3D approach is expected to be particularly beneficial. Volumetric recording of optical memory in glasses can achieve remarkable information densities, as was reported earlier in the case of picosecond [1] and femtosecond pulses [2–5]. However, so far, volumetric optical memories are considered impractical, partly due to the absence of a reliable readout mechanism, which requires at least a video-rate data-transfer speed.

Here, we discuss the 3D recording by dielectric breakdown, which can produce a read-only volumetric memory. The mechanism of dielectric breakdown was investigated for years theoretically [6] and experimentally [7]. However, a quantitative theory has not been developed so far, especially for the volumetric dielectric breakdown. The threshold of ablation, an inherently surface phenomenon, is much different from the in-bulk damage [8]. The main difference is due to the light-pulse self-action via the optical non-linear interaction with media, mainly the self-focusing [9] and spectral broadening [10], i.e. the white-light continuum (WLC) generation. Also, the results of the multi-shot optical damage threshold differ from that of a single shot. An additional issue exists in the definition of the damage threshold, e.g. a color-center formation has a different threshold from the structural damage such as a void or crack formation. Usually, the dielectric breakdown threshold is determined by the light intensity at which the electron density becomes critical (plasma reflection) for the wavelength of irradiation. The rationale of this is as follows: a highly absorbing state should be created inside a transparent dielectric via the non-linear light–matter interaction in order to trigger the breakdown. The amount of absorbed energy in the skin depth/volume is responsible for the recording of structural damage. This is a physically sound description of the breakdown, which was adopted for our study; moreover, it already explained quantitatively the results of ablation [11]. Recently, however, it was demonstrated by simulations that the approximately 100 times lower density was enough to make damage in the focal region inside silica [12].

In order to avoid as much as possible the effects related to pulse propagation (self-focusing), the focusing for recording should be carried out by a high numerical aperture objective lens, typically NA > 1, corrected for aberrations. At such conditions, the self-focusing power is higher than the threshold of observable damage, a bit/voxel. In this way, an intrinsic threshold of light-induced breakdown can be measured. We used this approach as described in detail in Sect. 2. In-

✉ Fax: +81-88/656-7598, E-mail: saulius@eco.tokushima-u.ac.jp

terestingly, for a similar focusing the threshold of dielectric breakdown in glass was found to be not dependent on the pulse duration in a span of 30 ps to 30 ns [13] and approximately equal to that of a 200 fs pulse in terms of irradiance. Obviously, further experimental and theoretical work are necessary to understand the variety of results on optically induced damage in the bulk.

As for the readout of volumetric memory, WLC generation is one of the alternatives to the reading by photoluminescence, scattering, or optical imaging. Here, we will not consider the WLC generation during the stage of bit recording, i.e. during the dielectric breakdown. Among the advantages of a WLC readout are its coherence with the excitation pulses and the relative ease of detection when a femtosecond high-frequency (80 MHz) excitation readout is employed. It is expected that the volumetric memory readout could utilize some of newly discovered features of WLC, e.g. the phase locking [14] or the enhancement of backward emission [15] in this fast-growing research field [16, 17].

The aim of this work was to compare experimental data of 3D optical recording by femtosecond pulses in glasses with theoretical predictions of dielectric breakdown [11]. The model incorporates the multi-photon absorption and avalanche ionization as the driving mechanisms of dielectric breakdown and was proven to describe successfully the ablation thresholds of metals and dielectrics. We propose the four-photon parametric interaction for optical memory readout. Measured transients of light emission from the recorded bits upon femtosecond excitation can be explained by the four-photon parametric interaction.

2 Experimental

The laser setup of optical memory recording was based on an oscillator (Tsunami) with a regenerative amplifier (Spitfire, Spectra Physics) and a three-axis piezostage (Polytec PI, Inc.) controlled by a computer. The pulse-energy stability was about 3% (r.m.s. value). The laser emission at 800 nm wavelength was focused into the sample by the infinity-corrected oil-immersion objective lens with a numerical aperture of NA = 1.35 and magnification ×100 using a microscope (Olympus IX70). The focusing of a Gaussian beam would correspond to a $D = K\lambda M^2/(2\mathrm{NA}) \simeq 0.48\ \mu\mathrm{m}$ diameter spot (FWHM) [19]; here $K = 1.07$ is the beam's truncation factor for a truncation ratio $T = 1.75$, λ is the wavelength, and $M^2 = 1.5$ is the beam-quality factor of Spitfire. The truncation ratio is defined as the Gaussian beam diameter at $1/\mathrm{e}^2$ divided by the diameter of the limiting aperture, $T = D_{\mathrm{beam}}/D_{\mathrm{Ap}}$. The waist length can be calculated as a doubled Rayleigh length $L = 2\pi\omega_0^2 M^2 M_{\mathrm{tr}}^2/\lambda \simeq 0.65\ \mu\mathrm{m}$, where $2\omega_0 = 1.27\lambda f/D_{\mathrm{beam}} \simeq 0.3\ \mu\mathrm{m}$ is the diffraction-limited waist diameter for a Gaussian beam focused by a lens with focal length $f = 1.8$ mm and M_{tr}^2 is an additional beam-quality factor relevant to the beam truncation [20]. $M_{\mathrm{tr}}^2 = D_{\mathrm{tr}}/D_0 \cong 2.38$, where $D_{\mathrm{tr}} = 1.725\lambda f/D_{\mathrm{Ap}}$ and $D_0 = 2\omega_0$ are diameters of the truncated and diffraction-limited Gaussian beams at $1/\mathrm{e}^2$ intensity, respectively. Thus, the approximate dimensions of the recording pulse, a 'light-pen' cross section, can be evaluated as (axial × lateral) $\simeq (0.48 \times 0.65)\mu\mathrm{m}^2$ for this non-paraxial focusing. The refractive index of glass at the wavelength of irradiation was calculated by the empirical Sellmeier formula for borosilicate glass BK7 (Schott), $\sqrt{\epsilon} = 1.51$ [21].

To evaluate a temporal fs pulse spread out after passing a microscope objective lens we have carried out a separate experiment. The pulse duration at different locations along the optical path and at the focus was measured by the GRENOUILLE technique [22] (Swamp Optics). This technique allows us to record a time × spectrum image of the pulse and, then, the pulse duration (FWHM) can be retrieved by the frequency-resolved optical gating (FROG) algorithm (Femtosecond Technologies). To measure the pulse duration at the focus, we used an additional solid-immersion lens [23], which collects strongly divergent light before introducing it into the GRENOUILLE setup (more details can be found in [24]). For all the retrieved pulse durations given in the text a FROG error was lower than 2%. The pulse duration of 130 fs was measured by GRENOUILLE at the output of the regenerative amplifier.

For the readout we used second- and third-harmonic generators (GWU, Spectra Physics) of fundamental oscillator (Tsunami) radiation. In the case of third-harmonic excitation, the readout was carried out by a fused-silica lens focusing ($f = 30$ mm) onto the area of recorded bits, while for a second-harmonic excitation a focusing in the microscope, the same as was implemented for the recording, was used. This allowed us to measure the readout from the individually addressed bits of 3D optical memory. The back-scattered emission from the bits was recorded on a spectrometer (SpectraPro 300i, Acton) equipped with a time-correlated single photon counting registration unit based on a microchannel plate photo-multiplier tube (R3809-50U, Hamamatsu) and a photon counting PC board (SPC300, BH Inc.) with time-deconvolution software (Edinburgh Inc.). The spectral resolution of the spectrometer (utilized as a monochromator in time-resolved measurements) was about 2 nm, narrower than the bandwidth of 10 nm (FWHM) of the fundamental emission of the fs laser. The temporal resolution of the SPC300 board was 13 ps. Such a setup can be seen as a prototype of a 3D optical memory write|read device, which is shown in Fig. 1. A dry objective lens could also be used as the recording and pickup head of 3D optical memory.

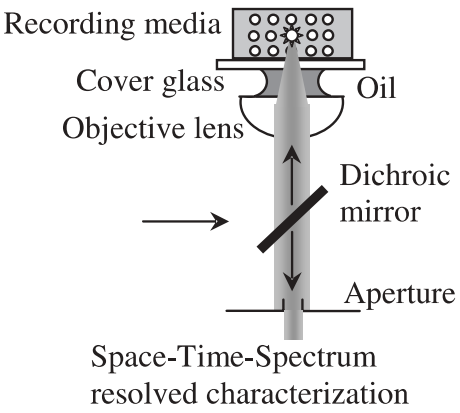

FIGURE 1 Principle of 3D optical memory recording and reading using fs pulses. A direct oil–sample contact is appropriate for a glass media, while a cover-glass spacer is necessary for polymers

3 Results and discussion

As a volumetric recording, here we consider a recording of optical memory achieved via dielectric/optical breakdown, which is localized in the bulk of transparent media, e.g. in glass [3, 5, 25, 26] or polymer [27, 28]. Customarily, the dielectric breakdown threshold (DBT) is defined by a free-carrier density, which corresponds to the plasma frequency at a given wavelength of recording. In order to photo-modify a transparent dielectric in the bulk, the energy large enough to cause a chemical bond breakage should be absorbed at the site (the voxel). Thus, when the electron density reaches the plasma density a dielectric turns into an absorbing material with the real part of the refractive index decreasing along with the increase in the free-carrier density, while the imaginary part increases [29], respectively. The absorption of an incident pulse takes place within the skin depth, which is less then 100 nm for a good conductor. The voxel of a cross section approximately equal to the skin depth is, thus, recorded and serves as a bit of 3D optical memory. Bits 2–3 times smaller in cross section than the focal spot can be recorded by fs pulses [5]. For the recording pulse energy of 1–2 DBT, the recorded bit in silica can be recognized in transmission as a light-scattering region, whose effective refractive-index change is about $(1-2)\times 10^{-3}$ [28] or by the absorption of dielectric breakdown induced defects, whose density can reach $10^{18}-10^{19}$ cm^{-3} [30, 31]. At higher recording irradiation intensity (starting at about 3 DBT) the void formation at the focus was accompanied with a surrounding cracking of glass. Those sub-micrometer cracks were found useful for a wet etching of 3D channels in silica [32, 33] due to the so-called stress corrosion effect [34]. Longer pulses cause an excess thermal load at the irradiation spot where they usually cause an extensive crack formation; hence, they are inappropriate for 3D recording. In polymethylmethacrylate, for example, the voids and open-core channels were recorded in bulk at an irradiance of 1–2 DBT [35].

3.1 *Dielectric breakdown*

Here, we will consider two major mechanisms of ionization in the laser field, which are most relevant to femtosecond dielectric breakdown: ionization by electron impact (avalanche ionization), and the multi-photon ionization. The following formula was successfully applied to describe ablation results [11] and, here, we adopt it for an in-bulk dielectric breakdown. The time dependence of the number density of free electrons n_e stripped off the atoms by these processes is defined by the rate equation [11]:

$$\frac{dn_e}{dt} = n_e w_{imp} + n_a w_{mpi} . \tag{1}$$

Here n_e is the electron density, n_a is the density of neutral atoms, w_{imp} is the time-independent probability (in [s^{-1}]) for the ionization by electron impact, and w_{mpi} is the probability for the multi-photon ionization. For the case of single ionization it is convenient to present the probabilities w_{mpi} and w_{imp} in the following form [36]:

$$w_{mpi} \approx \omega_0 n_{ph}^{3/2} \left(1.36\frac{\varepsilon_{osc}}{J_i}\right)^{n_{ph}} , \tag{2}$$

$$w_{imp} \approx \frac{\varepsilon_{osc}}{J_i}\left(\frac{2\,\omega_0^2 \nu_{eff}}{\omega_0^2+\nu_{eff}^2}\right) . \tag{3}$$

Here $\omega_0 = 2\pi c/\lambda$, ε_{osc} is the electron quiver energy in the laser field, n_{ph} is the number of photons necessary for atom ionization by the multi-photon process, which is the integer part of the quantity $(J_i/\hbar\omega_0)+1$, J_i is the ionization potential, and ν_{eff} is the effective collision frequency.

The general solution to (1) with the initial condition $n_e(t=0) = n_0$, where n_0 is the initial density of free electrons in the material, is the following:

$$n_e(I,\lambda,t) = \left\{n_0 + \frac{n_a w_{mpi}}{w_{imp}}\left[1-\exp\left(-w_{imp}t\right)\right]\right\}\exp\left(w_{imp}t\right) . \tag{4}$$

One can see from (2) and (3) that the relative role of the impact and multi-photon ionization depends dramatically on the relation between the electron quiver energy and the ionization potential.

If $\varepsilon_{osc} > J_i$ then $w_{mpi} > w_{imp}$, which is the case of high intensity (approximately at $I_l > 10^{14}$ W/cm^2) the multi-photon ionization dominates for any relationship between the frequency of the incident light and the efficient collision frequency. Such intensity is usually considered as the onset of multi-photon ionization via tunneling [37]. Multi-photon ionization dominates, and the number of free electrons increases linearly with time: $n_e \sim n_a w_{mpi} t$. The ionization time could be shorter than the pulse duration and the ionization threshold depends on the laser intensity I_l in [W/cm^2] and laser wavelength.

If $\varepsilon_{osc} \ll J_i$ and $\omega_0 \ll \nu_{eff}$, the electron-impact ionization is the main ionization mechanism, and one can neglect the second term in (1). The number of free electrons exponentially increases with the product of w_{imp} and the pulse duration: $n_e \propto n_0 \exp\left\{w_{imp} \times t_p\right\}$. Therefore in the long-pulse (ns) regime with much lower intensity the ionization threshold depends on the laser fluence $F = I \times t_p$.

It is generally accepted that the optical breakdown is achieved when the density of free electrons reaches the critical plasma density n_c for the incident laser wavelength λ:

$$n_c(\lambda)\left[\mathrm{cm}^{-3}\right] = \frac{\varepsilon_0 m_e \omega_0^2}{e^2} \cong \frac{1.1\times 10^{21}}{(\lambda\,[\mu\mathrm{m}])^2} , \tag{5}$$

where ε_0 is the permittivity of vacuum and m_e and e are the electron rest mass and charge, respectively. Above this electron density the laser light reflects from the created plasma and the laser–target coupling occurs through the electron thermal conductivity. Accordingly, $n_c = 1.74\times 10^{21}$ cm^{-3} at 800 nm wavelength.

Let us estimate the probability (in [s^{-1}]) and thus the ionization time, for each of the ionization mechanisms.

3.1.1 Multi-photon ionization. The oscillation energy of an electron in the field of the laser electromagnetic wave with the frequency ω_0 is expressed in the following way (in Gaussian units):

$$\varepsilon_{osc} = \frac{e^2 E^2}{4 m_e \omega_0^2} . \tag{6}$$

For practical use it is convenient to express it by using the definition of light intensity $I = c\sqrt{\epsilon}|\boldsymbol{E}|^2/(8\pi)$ (in SI units $I = \frac{1}{2}c\varepsilon_0\sqrt{\epsilon}|\boldsymbol{E}|^2$, where $\epsilon = (\mathrm{Re}(n))^2$ is defined by the real part of the refractive index, n, of the material):

$$\varepsilon_{\mathrm{osc}}\,[\mathrm{eV}] = (1+\alpha^2)\frac{e^2E^2}{4m\omega_0^2} = (1+\alpha^2)\frac{e^2}{4m\pi c^3}I\lambda^2 = (1+\alpha^2)\,9.34\,\frac{I}{10^{14}\,[\mathrm{W/cm^2}]}\left(\frac{\lambda}{[\mu\mathrm{m}]}\right)^2 , \quad (7)$$

here the factor $(1+\alpha^2)$ accounts for polarization of incident light with $\alpha = 0$ for linear and $\alpha = 1$ for circular. Combining (2) and (7), we present the probability of multi-photon ionization in the following convenient form:

$$w_{\mathrm{mph}}[\mathrm{s^{-1}}] = 1.88\times10^{15}\left(\frac{\lambda}{[\mu\mathrm{m}]}\right)^{2n_{\mathrm{ph}}-1} n_{\mathrm{ph}}^{3/2} \times\left[(1+\alpha^2)\frac{1.27\times10^{-13}I\left[\frac{\mathrm{W}}{\mathrm{cm^2}}\right]}{J_{\mathrm{i}}[\mathrm{eV}]}\right]^{n_{\mathrm{ph}}} . \quad (8)$$

Using (8), one can estimate the probability of multi-photon ionization in a SiO_2 target at the laser intensity of 6 TW/cm^2 with pulses of 800 nm wavelength and 200 fs duration (FWHM) taking into account the ionization potential of Si (8.15 eV [38]), since that of O is larger (13.62 eV [38]). The intensity of about 6.6 TW/cm^2 is typical for the light-induced dielectric breakdown threshold in borosilicate and silica glass and can be considered as a recording intensity of 3D optical memory. One can then find $w_{\mathrm{mpi}} \simeq 1.59\times10^9\ \mathrm{s^{-1}}$ at 800 nm wavelength for linearly polarized light.

3.1.2 Avalanche ionization by electron impact. The energy of an electron accelerated by the laser electric field can be calculated as:

$$\frac{\mathrm{d}\varepsilon_e}{\mathrm{d}t} = \Delta\varepsilon\cdot\nu_{\mathrm{ea}} . \quad (9)$$

Here $\Delta\varepsilon$ is the average energy gained by an electron as a result of a single collision,

$$\Delta\varepsilon = \frac{2\varepsilon_{\mathrm{osc}}\omega_0^2}{\omega_0^2+\nu_{\mathrm{ea}}^2} ; \quad (10)$$

ν_{ea} is the average over the electron spectrum collision frequency between electrons and atoms in the target, which can be determined for the particular target material with the help of the Boltzmann transport equation for the entire range of electron energies. A reasonable estimate for the collision frequency $\nu_{\mathrm{ea}} \sim 6\times10^{14}\ \mathrm{s^{-1}}$ is given in [36]; it is independent of the electron energy. Taking the given value one can conclude that the average energy gain per collision is approximately $\Delta\varepsilon \cong 2\varepsilon_{\mathrm{osc}}$. As (9) suggests, the electron energy grows linearly with time: $\varepsilon_{\mathrm{e}} = \Delta\varepsilon\,\nu_{\mathrm{ea}}t$. Making use of (10), one obtains for the energy gain:

$$\varepsilon_{\mathrm{e}}\,[\mathrm{eV}] \cong 112\times I\left[\frac{\mathrm{W}}{\mathrm{cm^2}}\right]\times\lambda^2[\mu\mathrm{m}]\times t\,[\mathrm{s}] . \quad (11)$$

Thus the time t_{ion} required for an electron to gain an energy equal to the ionization potential (the ionization time) is:

$$t_{\mathrm{ion}} = w_{\mathrm{imp}}^{-1} \approx \frac{J_{\mathrm{i}}}{\Delta\varepsilon\nu_{\mathrm{ea}}} = \frac{J_{\mathrm{i}}}{112\times I\left[\frac{\mathrm{W}}{\mathrm{cm^2}}\right]\times\lambda^2\,[\mu\mathrm{m}]} . \quad (12)$$

Following (12), the probability of the avalanche ionization of SiO_2 with 800 nm wavelength, 200 fs pulses at the laser intensity of 6.6 TW/cm^2 is $w_{\mathrm{imp}} = 4.96\times10^{13}\ \mathrm{s^{-1}}$.

3.2 *Recording by dielectric breakdown*

Let us apply the formulae of Sect. 3.1 to the particular case of optical three-dimensional recording in glass. As a DBT we consider the intensity at which the free electron plasma density is attained. Also, let us implement a Gaussian intensity distribution $I(t) = I_0\exp\left[-4\ln2((t-t_0)/t_{\mathrm{p}})^2\right]$ for calculations using (4), (8), and (12) with $t_{\mathrm{p}} = 200$ fs being the pulse duration at full-width at half maximum (FWHM). A typical value of free electrons in dielectrics such as SiO_2 is $n_0 = 10^{14}\ \mathrm{cm^{-3}}$; in fact, we have checked that the maximum electron density was not sensitive to the initial concentration as long as it was below $10^{15}\ \mathrm{cm^{-3}}$. Also, we consider an ionization of only Si, which has the lower ionization potential. Thus, an available atomic number density for excitation is only 1/3 of that of glass, which is $n_{\mathrm{a}} = 2.2\times10^{22}$ for SiO_2 ($n_{\mathrm{a}} = \varrho N_{\mathrm{A}}/M$, where $\varrho \simeq 2.2\ \mathrm{g/cm^3}$ is the density, $M = 60.09$ g is the atomic mass, and $N_{\mathrm{A}} = 6.02\times10^{23}$ is the Avogadro number). The results of simulation are shown in Fig. 3 for the Gaussian and step-like excitation profiles. The calculated free-carrier density at the maximum of a 6 TW/cm^2 pulse was much higher than the total number density of available Si atoms $n_{\mathrm{a}}/3$, while for 3.5 TW/cm^2 the critical plasma density was just reached. For the 6 TW/cm^2 irradiance the critical plasma density was surpassed for approximately the duration of the pulse according to simulations (Fig. 2). For the ionization potential of oxygen and the corresponding number density $2n_{\mathrm{a}}/3$ one would find only $n_{\mathrm{e}} = 1.47\times10^{19}\ \mathrm{cm^{-3}}$ at the maximum of the 6 TW/cm^2 pulse, which is much lower than the critical density.

Experimentally, a 6.6 TW/cm^2 DBT inside fused silica at 10 μm depth, where the aberrations [39] were minimal for our recording conditions, was found. At this irradiance the critical density was surpassed for the approximate pulse duration according to the simulations given above. The theoretical threshold at which the critical density was reached at

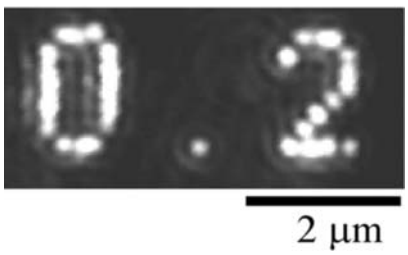

FIGURE 2 Image of a 'bit' pattern recorded in the volume of silica at 10 μm depth by 150 fs pulses of 800 nm wavelength focused with a NA = 1.4 objective lens [5]. Imaging (the readout) wavelength was 488 nm. The distance between adjacent bits was 0.2 μm

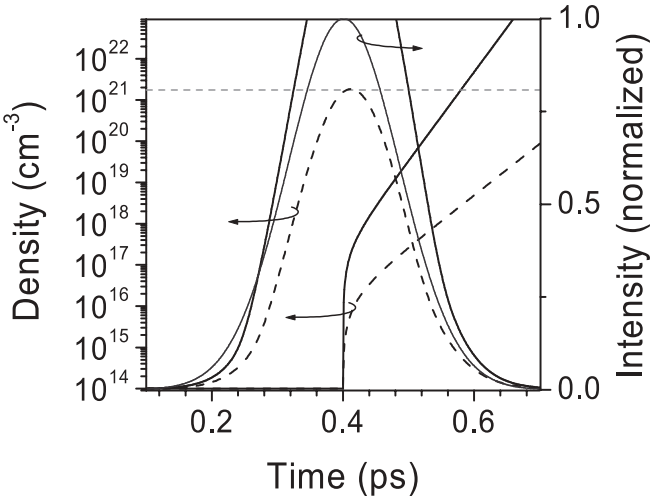

FIGURE 3 Electron-density time evolution for Gaussian and step-like excitation (*left-hand axis*). Gaussian profile of the pulse is given on the *right-hand axis*. Critical plasma density for 0.8 μm wavelength is 1.74×10^{21} cm^{-3} (*gray horizontal line*). The *solid* and *dashed* density profiles were calculated for the 6- and 3.5 TW/cm^2 intensities, respectively. Collision frequency $\nu_{ea} = 6 \times 10^{14}$ s^{-1} [36]

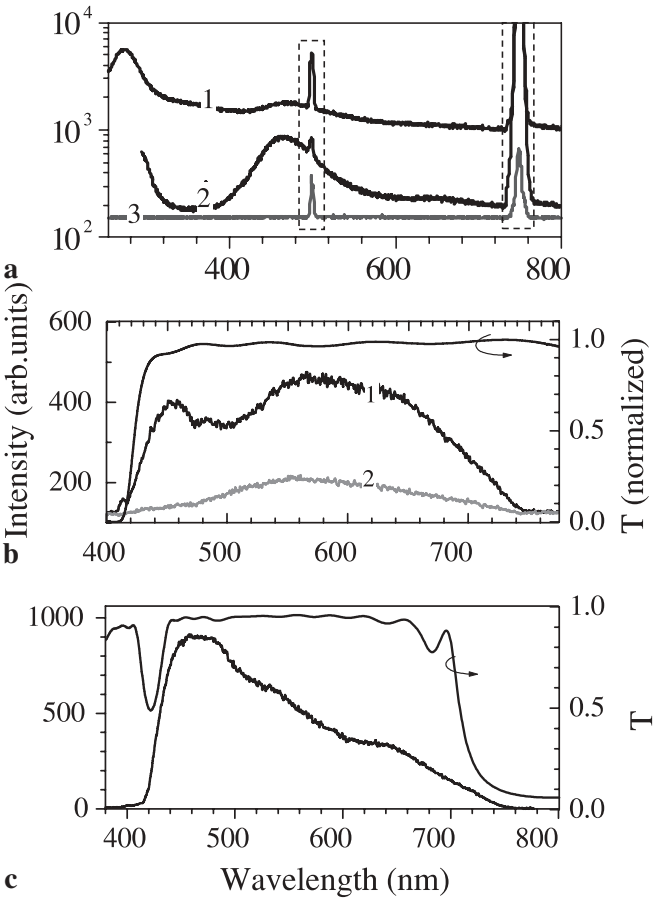

FIGURE 4 Spectra of emission from the area of bits excited by 250 nm wavelength (**a**) and from a single bit excited by 400 nm (**b**) and 800 nm (**c**), respectively. **a** Curve 1 shows unfiltered, curve 2 long-pass (> 370 nm) filtered emission, and curve 3 that from bits-free region. **b** Curve 1 depicts emission from a single bit, and curve 2 from an undamaged region. Transmission profiles of dichroic mirrors (see Fig. 1) are given in **b** and **c**. *Boxed regions* mark second and third orders of excitation at 253 nm

the maximum of the intensity envelope comprises 53% of the experimentally observed threshold.

Also, the linear dependence of the DBT on the wavelength predicted by the theory given above [11] was confirmed experimentally [40] for the 400–800 nm wavelength region. As a conclusion of this part we can state that the calculations presented above can qualitatively well explain the experimentally measured value of the DBT. The theoretical approach utilized here considers explicitly the light–solid matter interaction, which is not the case for the Keldysh theory [6] as was pointed out recently [41]. In other works [8, 12] the photo-ionization rate was calculated directly from the Keldysh theory [6], while here we used the ionization probabilities derived in [36].

3.3 *Readout of optical memory*

The bit-readout experiments were carried out by measuring light-emission spectra Fig. 4 and their transients (Figs. 5 and 6) at different excitation wavelengths from the area of recorded bits as well as from the individual bits in silica. For excitation of bit emission we used fundamental, second-, and third-harmonic radiation of a fs-laser source. The readout pulse intensity was calculated from a direct measurement of pulse energy at the focus by using a solid-immersion lens [23] and was kept lower than 10 GW/cm^2 in all experiments. Thus, secondary optical damage was avoided and the observed light emission was not caused by the breakdown plasma radiation, which usually accompanies the optical damage [42].

A spectrally broad-band emission was observed from the bits (Fig. 4) upon excitation by femtosecond pulses. Time-integrated spectra had signatures of photo-luminescence (PL) bands typical for defects in silica. For example, PL at 280 nm and 470 nm is related to the oxygen vacancy, V_O, while the 650 nm band is the signature of a non-bridging oxygen hole center (NBOHC) as we reported earlier [43, 44]. Interestingly, an up-conversion type of emission was observed at a 800 nm readout of the bit (Fig. 4c). Such an emission can be caused by multi-photon excitation of silica or by parametric four-beam interaction (Sect. 3.3.3).

In order to distinguish between coherent WLC emission and PL we carried out time-resolved measurements at different spectral windows of registered emission (Fig. 5). Exponential time decay with a 3.7 ns constant was found at 280 nm, which is typical for a V_O defect. Apart from PL transients, a coherent peak appeared in the recorded emissions (within our temporal resolution of about 20 ps). To avoid detection of the Rayleigh scattering of the readout pulse we used a 2 nm bandpass monochromator slit, which is several times narrower than the bandwidth of the excitation pulse. Also, we have observed similar coherent WLC spikes in the emission from single bits excited by 400 nm pulses in a microscope (Fig. 6). These observations along with a sharp edge of the emission at 400 nm (Fig. 4c) upon excitation at 800 nm allowed us to suggest that a non-linear mechanism of WLC was responsible for the emission, as the following discussion shows.

3.3.1 Light emission from the bits. White-light continuum is typically observed in transparent dielectrics (crystals and

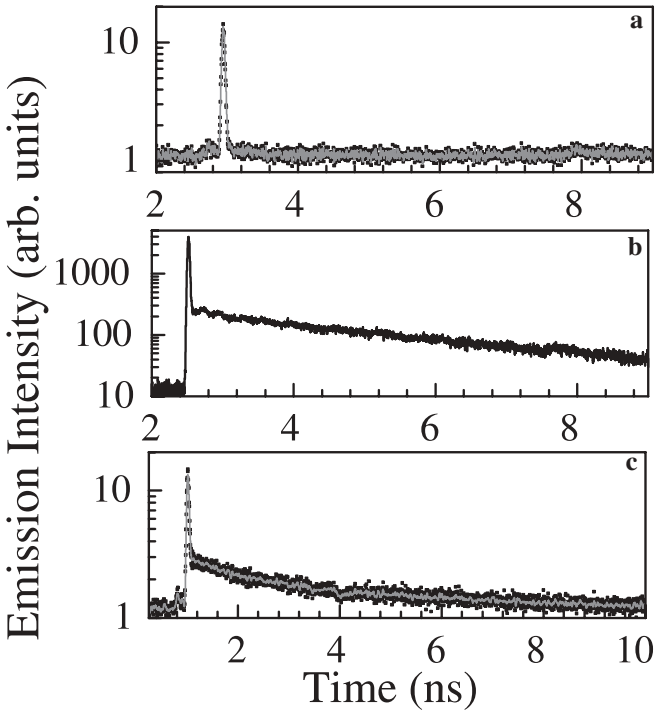

FIGURE 5 Transients of WLC at 253 nm (**a**), 280 nm (**b**), and 570 nm (**c**). An area of bits recorded in silica at 10 μm depth was irradiated by 150 fs pulses of 253 nm wavelength (third harmonic of 760 nm emission) and imaged onto spectrometer slit. Separation between excitation pulses was 24 ns

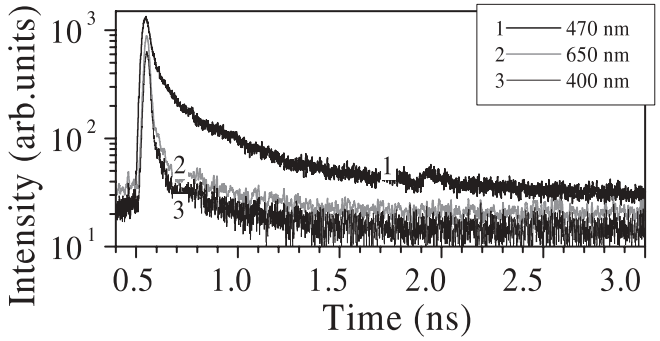

FIGURE 6 Transients of WLC from a single bit at different wavelengths. Monochromator slit corresponded to a 2 nm spectral width

glasses) at about 10^{11} W/cm^2 irradiance; for example, in BK7 and silica WLC was observed at $(4-5)\times 10^{11}$ W/cm^2 irradiance at 800 nm wavelength.

Two mechanisms of coherent WLC emission should be considered in the case of fs excitation: self-phase modulation (SPM) and four-photon parametric interaction. The former propagates axially along the excitation, while the latter spreads over the cone. Both mechanisms are related to the $\chi^{(3)}$ non-linearity.

3.3.2 Spectral broadening via self-phase modulation. Let us evaluate a spectral broadening of a Gaussian beam due to SPM after passing a high-intensity focal region at the irradiance close to the dielectric breakdown. The DBT in silica was found at the irradiance $I_{\mathrm{DBT}} = 6.6\times 10^{12}$ W/cm^2 for $t_\mathrm{p} = 200$ fs pulses (pulse duration was measured by the GRENOUILLE technique as described in Sect. 2) with Rayleigh length $z_\mathrm{R} \simeq 0.7$ μm. The non-linear refractive index of silica is $n_2 = 2.5\times 10^{-16}$ cm^2/W [45], where the intensity-dependent refractive index is given by $n(I) = n_0 + n_2 I$. The cause of spectral broadening is the phase change of the passing pulse [37]. According to the classical theory [37], the distance over which the phase is changed by 1 rad is called the non-linear length and is given by $L_\mathrm{nonl} = ((2\pi/\lambda)n_2 I)^{-1} = 77$ μm for I_{DBT}. Then, the maximum shift of the frequency, which is the same for the Stokes and anti-Stokes modes, is given by $\Delta\omega = \sqrt{2/\mathrm{e}}\,\varphi_\mathrm{max}\Delta\omega_0 = 1.9$ cm^{-1}, where the maximum phase shift is $\varphi_\mathrm{max} = (2\pi/\lambda)n_2 I\cdot 2z_\mathrm{R}$ and the spectral width at intensity (e^{-2}) level is $\Delta\omega_0 = 260$ cm^{-1} (10 nm FWHM spectral bandwidth at $\lambda = 800$ nm). The spectral shift of $\Delta\omega = 1.9$ cm^{-1} is small, indeed, for our pulses of $\omega_0 = 12\,500$ cm^{-1} ($\lambda = 800$ nm).

The theory of SPM [37], which accounts for self-steepening of the pulses, predicts even smaller spectral broadening after passing a focal region due to a small parameter $Q = 2z_\mathrm{R}n_2 I/(c(2\sqrt{\ln 2})t_\mathrm{p}) \ll 1$ for the conditions considered above. Indeed, Stokes and anti-Stokes spectral shifts are given by $\Delta\omega_{\mathrm{s,a}} = \omega_0\left(0.25(\sqrt{Q^2+4}\mp Q) - 0.5\right) < 1$ cm^{-1} at the dielectric breakdown irradiance. This suggests that according to the classical WLC generation models the experimentally observed spectral broadening could not be accounted for by SPM due to a short length of propagation inside a region of high light intensity [24].

3.3.3 Spectral broadening via four-photon parametric interaction. Let us consider the four-photon parametric interaction [46] as the mechanism of spectral broadening observed experimentally. For a single, intense, and monochromatic coherent light wave interacting with a transparent non-resonant medium a third-order non-linear parametric process, such as shown in Fig. 7a, should be considered for WLC generation. Conservation of energy and momentum of the interacting photons is given by:

$$\begin{cases} 2\omega_0 = \omega_1 + \omega_2, \\ 2\boldsymbol{k}_0 = \boldsymbol{k}_1 + \boldsymbol{k}_2, \end{cases} \tag{13}$$

where $\hbar\omega_i$ and $k_i = 2\pi/\lambda_i$ $(i = 1, 2)$ are the energy and wavevector of the interacting photons, respectively. Many combinations of $(\boldsymbol{k}_1; \boldsymbol{k}_2)$ vector pairs satisfy the conditions given by (13). From the energy conservation it follows that $2/\lambda_0 = \lambda_1^{-1} + \lambda_2^{-1}$; hence, the blue-shifted emission should not be shorter than $\lambda_0/2$. We, indeed, have observed such a blue cutoff at 400 nm for an emission excited by 800 nm wavelength (Fig. 4c). A phase-matching condition imposes the following relations:

$$\begin{cases} \dfrac{n(\lambda_1)}{\lambda_1}\cos\theta_1 + \dfrac{n(\lambda_2)}{\lambda_2}\cos\theta_2 = \dfrac{2n(\lambda_0)}{\lambda_0}, \\ \dfrac{n(\lambda_1)}{\lambda_1}\sin\theta_1 = \dfrac{n(\lambda_2)}{\lambda_2}\sin\theta_2, \end{cases} \tag{14}$$

where $n(\lambda)$ represents the dispersion of the material. The solution of (14) is shown in Fig. 7b for the case of borosilicate glass BK7 (Schott), whose room-temperature dispersion

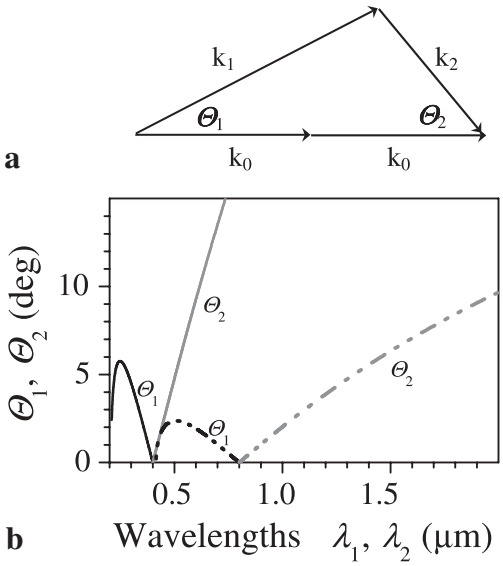

FIGURE 7 **a** Phase-matching condition of four-photon parametric interaction. **b** Wavelength–angle dependence of coherent emission for $\lambda_0 = 0.4$ μm (*solid lines*) and 0.8 μm (*dashed*) respectively

was calculated by the empirical Sellmeier formula [37]. As one can see, the angles $\theta_{1,2}$ are small, $< 5°$, for the parametric emission at the wavelengths around that of the excitation $\lambda_{ex} : \lambda_{ex}/2 < \lambda_{ex} < 2\lambda_{ex}$. Parametric emission is propagating conically along the direction of the driving excitation (Fig. 7). When there are no recorded bits the WLC, even if present, would escape detection in our setup, which records the back-scattered and emitted light (Fig. 1). The presence of a bit changes locally the optical properties and, most importantly, acts as a scattering point of WLC and PL. This makes it possible to recognize (to read out) the bit by those signatures of WLC, PL, Rayleigh scattering, and transmission imaging. All these methods could, in fact, be used as the readout mechanisms of 3D optical memory. A high numerical aperture lens used for the readout ensures effective detection of emission spread over large angles. Indeed, a cone angle at the focus of a NA = 1.35 objective lens is about 126 degrees.

Further studies are necessary to elucidate the details of a WLC readout mechanism. Namely, the electrical field enhancement effect at the bit can play an important role; $\chi^{(3)}$ at the optically modified region of the bit should be established in order to evaluate the efficiency of such readout. Also, the long-term stability of 3D optical memory in glasses, as well as the cross-talk issues in the readout of 3D memory [47] need more studies aiming at implementation into viable applications. Here, we have focused on the proof of the principle that a WLC could be used for the readout of 3D optical memory.

4 Conclusions

3D optical memory recording by fs pulses can be explained by the model of dielectric breakdown developed for the ablation. The experimentally observed threshold of the in-bulk dielectric breakdown of silica was reproduced numerically by implementing the ionization potential of Si for calculations. As a readout mechanism of 3D memory we propose a non-linear four-beam parametric interaction, which was observed in the emission from the bits during excitation by fs pulses.

ACKNOWLEDGEMENTS This work was partially supported by the Satellite Venture Business Laboratory (SVBL) of the University of Tokushima and the Contract No. F62562-03-P-0208 AOARD 02-35 of the Asian Office of Air Force Research and Development. A.V.R. acknowledges a grant for the scientific visit of SVBL.

REFERENCES

1 H. Misawa: Electronics Weekly (UK) **5**, 10 (1995)
2 E.N. Glezer, M. Milosavljevic, L. Huang, R.J. Finlay, T.-H. Her, J.P. Callan, E. Mazur: Opt. Lett. **21**, 2023 (1996)
3 M. Watanabe, H. Sun, S. Juodkazis, T. Takahashi, S. Matsuo, Y. Suzuki, J. Nishii, H. Misawa: Jpn. J. Appl. Phys. **37**, L1527 (1998)
4 J. Qiu, K. Miura, H. Inouye, J. Nishii, K. Hirao: Nucl. Instrum. Methods Phys. Res. B **141**, 699 (1998)
5 S. Juodkazis, T. Kondo, V. Mizeikis, S. Matsuo, H. Misawa, E. Vanagas, I. Kudryashov: in *Proc. Bi-lateral Conf. Optoelectronic and Magnetic Materials*, Taipei, ROC, 25–26 May 2002, pp. 27–29 [available as arXiv: physics/0205025 v1 9 May 2002]
6 L.V. Keldysh: Sov. Phys. JETP **20**, 1307 (1965)
7 N. Blombergen: IEEE J. Quantum Electron. **QE-10**, 375 (1974)
8 A.-C. Tien, S. Backus, H. Kapteyn, M. Murnane, G. Mourou: Phys. Rev. Lett. **82**, 3883 (1999)
9 D. von der Linde, H. Schuler: J. Opt. Soc. Am. B **13**, 216 (1996)
10 O.M. Efimov, S.V. Garnov, L.B. Glebov, K. Gabel, S. Grantham, M. Richardson, M.J. Soileau: J. Opt. Soc. Am. B **15**, 193 (1998)
11 E.G. Gamaly, A.V. Rode, B. Luther-Davies, V.T. Tikhonchuk: Phys. Plasmas **9**, 949 (2002)
12 L. Sudrie, A. Couairon, M. Franco, B. Lamouroux, B. Prade, S. Tzortzakis, A. Mysyrowicz: Phys. Rev. Lett. **89**, 186 601 (2002)
13 O.M. Efimov, V.S. Popikov, M.J. Soileau: J. Opt. Technol. **63**, 120 (1996)
14 M. Bellini, T.W. Hänsch: Opt. Lett. **25**, 1049 (2000)
15 J. Yu, D. Mondelain, G. Ange, R. Volk, S. Niedermeier, J.P. Wolf, J. Kasparian, R. Sauerbrey: Opt. Lett. **26**, 533 (2001)
16 A.L. Gaeta: Opt. Lett. **27**, 924 (2002)
17 A.M. Zheltikov: Phys. Usp. **45**, 687 (2002)
18 E.G. Gamaly, A.V. Rode, B. Luther-Davies: Appl. Phys. A **69**, S121 (1999)
19 P. Belland, J. Crenn: Appl. Opt. **21**, 522 (1982)
20 H.-Y. Sun: Opt. Eng. **37**, 2906 (1998)
21 M. Bass (ed.): *Handbook of Optics: Devices, Measurements, and Properties*, Vol. 2 (McGraw-Hill, New York 1995)
22 P. O′Shea, M. Kimmel, X. Gu, R. Trebino: Opt. Lett. **26**, 932 (2001)
23 S. Matsuo, H. Misawa: Rev. Sci. Instrum. **73**, 2011 (2002)
24 S. Juodkazis, T. Kondo, S. Dubikovski, V. Mizeikis, S. Matsuo, H. Misawa: In: Proc. SPIE, Advanced Laser Technologies ALT-02 (2003) in press
25 M. Watanabe, S. Juodkazis, H. Sun, S. Matsuo, H. Misawa, M. Miwa, R. Kaneko: Appl. Phys. Lett. **74**, 3957 (1999)
26 M. Watanabe, S. Juodkazis, H. Sun, S. Matsuo, H. Misawa: Appl. Phys. Lett. **77**, 13 (2000)
27 K. Yamasaki, S. Juodkazis, M. Watanabe, H. Sun, S. Matsuo, H. Misawa: Appl. Phys. Lett. **76**, 1000 (2000)
28 K. Yamasaki, S. Juodkazis, T. Lippert, M. Watanabe, S. Matsuo, H. Misawa: Appl. Phys. A **76**, 325 (2003)
29 H. Misawa, S. Juodkazis, A. Marcinkevicius, M. Watanabe, V. Mizeikis, S. Matsuo: In: Laser Applications in Microelectronic and Optoelectronic Manufacturing VI, ed. by M.C. Gower, H. Helvajian, K. Sugioka, J.J. Dubowski (publisher SPIE **4274**) (SPIE, Bellingham, WA, USA 2001) pp. 98–109
30 H. Misawa, H. Sun, S. Juodkazis, M. Watanabe, S. Matsuo: In: Laser Applications in Microelectronic and Optoelectronic Manufacturing V, ed. by H. Helvajian, K. Sugioka, M.C. Gower, J.J. Dubikowsky (publisher SPIE **3933**) (SPIE, Bellingham, WA, USA 2000) pp. 246–260

31 S. Juodkazis: Lithuanian J. Phys. **42**, 119 (2002)
32 A. Marcinkevicius, S. Juodkazis, M. Watanabe, M. Miwa, S. Matsuo, H. Misawa, J. Nishii: Opt. Lett. **26**, 277 (2001)
33 S. Juodkazis, K. Yamasaki, A. Marcinkevicius, V. Mizeikis, S. Matsuo, H. Misawa, T. Lippert: In: Mater. Res. Soc. Symp. Proc. Vol. 687, 2002, pp. 173–178
34 S.M. Wiederhorn: J. Am. Ceram. Soc. **50**, 407 (1967)
35 K. Yamasaki, S. Juodkazis, T. Lippert, M. Watanabe, S. Matsuo, H. Misawa: Appl. Phys. A **76**, 325 (2003)
36 Y. Raizer: *Gas Discharge Physics* (Springer, Berlin, Heidelberg 1991)
37 S.A. Achmanov, V.A. Vyslouch, A.S. Chirkin: *Optics of Femtosecond Laser Pulses* (Nauka, Moscow 1988)
38 R.C. Weast (ed.): *Handbook of Chemistry and Physics*, 69th edn. (CRC, Boca Raton, FL 1988)
39 A. Marcinkevicius, V. Mizeikis, S. Juodkazis, S. Matsuo, H. Misawa: Appl. Phys. A **76**, 257 (2003)
40 S. Juodkazis, M. Horyama, M. Miwa, M. Watanabe, A. Marcinkevicius, V. Mizeikis, S. Matsuo, H. Misawa: in *Proc. 7th Int. Conf. Laser and Laser-Information Technologies*, Ed. by V.Y. Panchenko, V.S. Golubev (publisher SPIE **4644**) (SPIE, Bellingham, WA, USA 2002) pp. 27–38
41 C.B. Schaffer, A. Brodeur, E. Mazur: Meas. Sci. Technol. **12**, 1784 (2001)
42 S. Juodkazis: Res. Adv. Appl. Phys. **2**, 45 (2001)
43 M. Watanabe, S. Juodkazis, H. Sun, S. Matsuo, H. Misawa: Phys. Rev. B **60**, 9959 (1999)
44 S. Juodkazis, M. Watanabe, H. Sun, S. Matsuo, J. Nishii, H. Misawa: Appl. Surf. Sci. **154–155**, 696 (2000)
45 A.A. Zozulya, S.A. Diddams, T.S. Clement: Phys. Rev. A **58**, 3303 (1998)
46 G.S. He, S.H. Liu: *Physics of Nonlinear Optics* (World Scientific, London 1999)
47 M. Watanabe, S. Juodkazis, S. Matsuo, J. Nishii, H. Misawa: Jpn. J. Appl. Phys. **39**, 6763 (2000)